SeaTwirl's wind farm layouts analysis

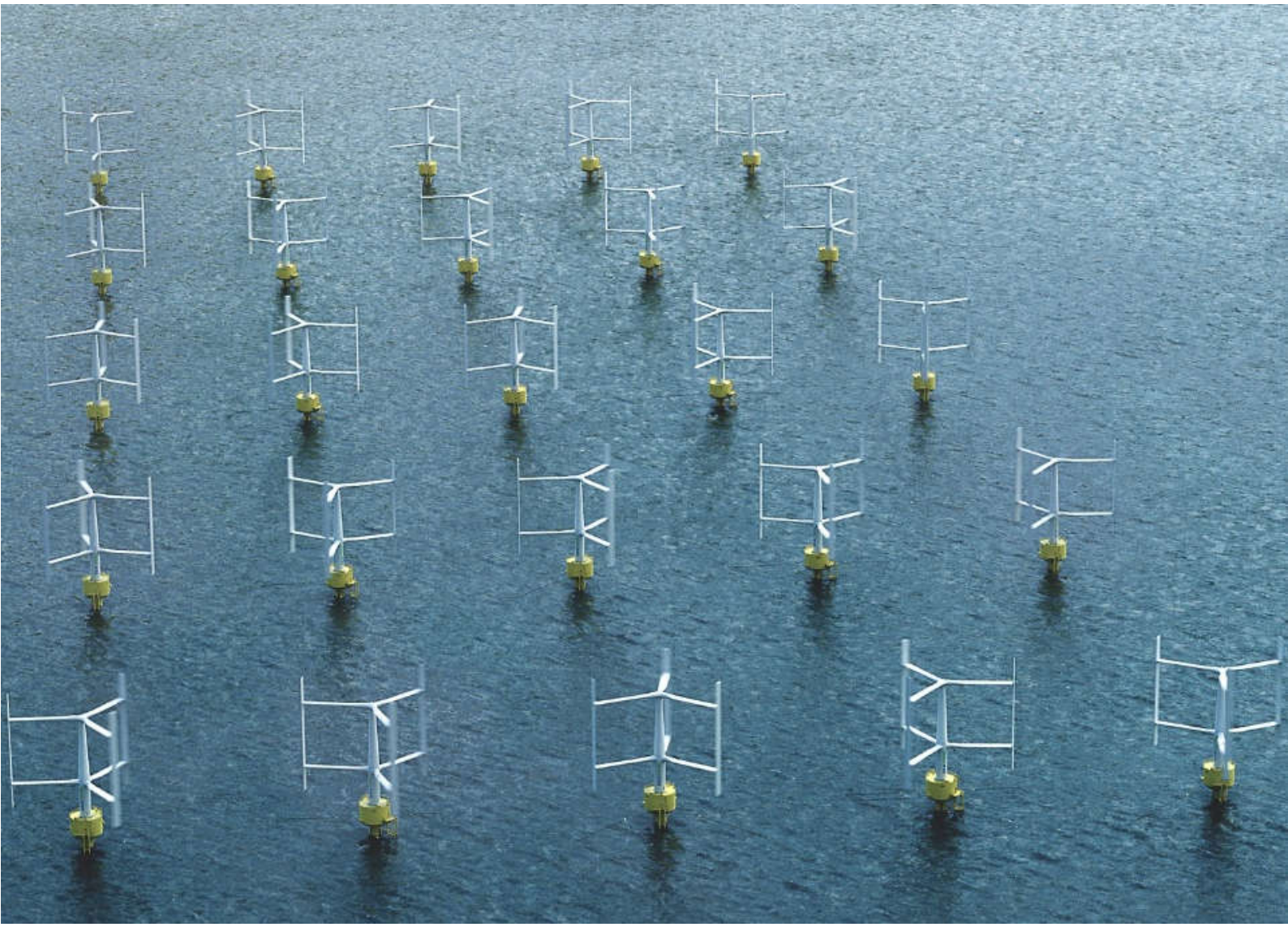

Report developed by Dr Pablo Ouro, Senior CFD consultant

Prepared for:

SeaTwirl AB

Lilla Bommen 1, floor 13,

411 04 Göteborg (Sweden)

+46 (0)705-85 77 48

Prepared by:

Dr Pablo Ouro

Senior CFD consultant

19 Melrose Gardens, Cardiff, UK.

T: +44 (0)7462280205

E: pablo.ouro@manchester.ac.uk

Abstract

This report presents estimates of the energy generation from wind farms comprising 25 10MW vertical axis turbines using SeaTwirl's design. Comparisons with analogous farms adopting 10MW horizontal axis turbines show that the former yield notably higher energy generation due to reduced wake effects. The presented results outline that the aspect ratio of the vertical axis turbine rotor is essential to increase their performance.

1. Background information

Offshore wind farms consider the deployment of several turbines in multiple rows in order to make the most use of the consented sea region. Discarding restrains due to bathymetry features, the best wind farm layout needs to balance the increase in costs from cabling or moorings when turbine spacing is large, with the consequent reduction of wake effects that can decrease the energy yield when turbines are in close proximity.

2. Wake modelling

The wake developed behind wind turbines is highly complex, characterised by a region of low velocity behind the rotor that eventually recovers the free-stream velocity further downwind. This recovery depends on the acting thrust of the turbine as well as the turbulence intensity of the oncoming wind. To date, most research characterising the wind turbine wakes focused almost exclusively on horizontal axis turbines (HAT) as they dominate the market. These wakes can be reasonably well represented in their time-averaged sense using analytical wake models based on either experimental or field data or high-fidelity simulations. Ouro and Lazennec (2021) developed the first analytical wake model for vertical axis turbines (VAT) considering their geometric and operational particularities, which was well validated against high-fidelity simulations.

The first models considered a so-called "top-hat" velocity deficit distribution as proposed by Jensen and then by Jansen but this approach failed to represent the wake shape. More recently, Gaussian wake models provide a notable improvement as they conserve mass and momentum together with capturing the wake shape over its cross-section and in the downwind direction. Equation (1) presents how the velocity wake deficit (defined as the difference between velocity decay in the wake region and that in the free-stream) for a HAT (ΔU_H) has two components, one accounting for velocity deficit magnitude (C_H) that depends on the thrust coefficient (C_T) and wake expansion (σ_H, Eq. (2)) and its shape (f_H) which has an exponential distribution in the radial direction. It is important to note that the wake expansion is a linear function that scales with k_H known as the wake expansion rate that is $k_H = 0.35 \cdot I_u$, with I_u denoting turbulence intensity. Thus, higher turbulence intensity levels (normally occurring at low velocities) leads to a faster wake recovery.

$$\Delta U_H = C_H(x)\ f_H(y,z) = \left(1 - \sqrt{1 - \frac{C_T}{8\tilde{\sigma}_H^2}}\right) \exp\left(-\frac{y^2+z^2}{2\tilde{\sigma}_H^2}\right) \tag{1}$$

$$\tilde{\sigma}_H(\tilde{x}) = k_H^*\ x + \varepsilon_H \tag{2}$$

The shape of the wakes developed behind HATs and VATs are depicted in Figure 1. This shows that a Gaussian model provides a physically sound representation of the HAT wake as only the rotor diameter is the scaling geometry feature with a circular cross-section. Conversely, VATs have a rectangular cross-section with their diameter (D) and height (H) meaning that the wake shape over the vertical and horizontal planes differ, with Gaussian models failing to capture this. Ouro and Lazennec (2021) proposed an anisotropic super-Gaussian model that allows to represent with a super-Gaussian distribution the wake distribution over the two spatial directions independently, i.e. $\Delta U_V(z)$ and $\Delta U_V(y)$. Considering the aspect ratio ξ = H/D, the super-Gaussian VAT wake model reads:

$$\begin{aligned}\Delta U_V &= C_V(x)\ \exp\left(-\frac{y^{n_y}}{2\sigma_{V_y}^2}\right)\ \exp\left(-\frac{z^{n_z}}{2\sigma_{V_z}^2}\right) \\ &= \left(2^{\gamma-1} - \sqrt{2^{\gamma-2} - \frac{C_T}{8\ \sigma_{V_y}^{2/n_y}\ \sigma_{V_z}^{2/n_z}\ \Gamma(1/n_y)\ \Gamma(1/n_z)}}\right)\ \exp\left(-\frac{y^{n_y}}{2\sigma_{V_y}^2} - \frac{z^{n_z}}{2\sigma_{V_z}^2}\right)\end{aligned} \tag{3}$$

$$\begin{aligned}\tilde{\sigma}_{V_y} &= k_{V_y}^* x + \varepsilon_{V_y} \\ \tilde{\sigma}_{V_z} &= k_{V_z}^*\ x/\xi + \varepsilon_{V_z}\end{aligned} \tag{4}$$

$$\varepsilon_{V_y} = \varepsilon_{V_z} = \left(\frac{C_T n_y n_z}{2^{\gamma+3}\Gamma(1/n_y)\ \Gamma(1/n_z)}\right)^{\gamma/2} \tag{5}$$

The wake expansion rates k_{Vy} and k_{Vz} are equal to $0.50 \cdot I_u$ and ε_V denotes the wake width at the onset of the wake. Note that the super-Gaussian exponents are $n_y = 0.95 \cdot e^{-0.35x}$ and $n_z = 4.50 \cdot e^{-0.70x}$ which evolve over the downwind direction so does the wake shape as it starts with a more rectangular (top-hat) shape and eventually converging to a Gaussian shape further downstream (usually after 10-12 turbine rotor diameters).

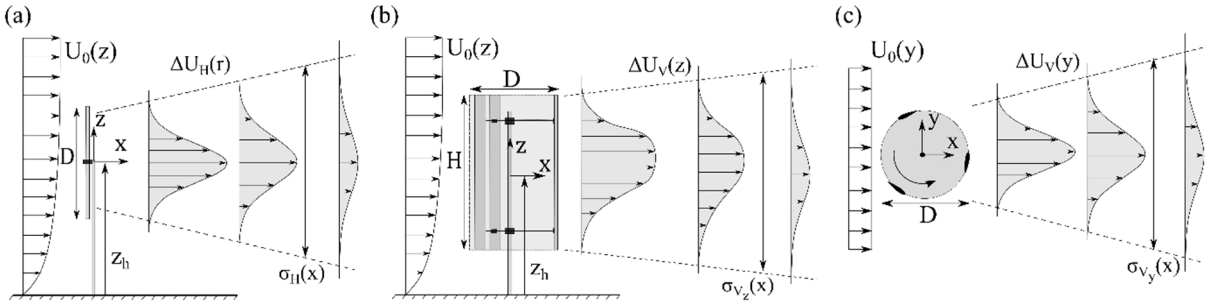

Figure 1 Velocity deficit distribution downstream of a HAT (a) and a VAT (b and c)

Turbine wakes are well-defined by these models, but when deployed in farms there are wakes that overlap one another. For instance, Figure 2 shows a small farm with three rows of four turbines in close proximity. To account for this, we adopt a linear superposition models that sums the velocity deficit from several wakes at any location.

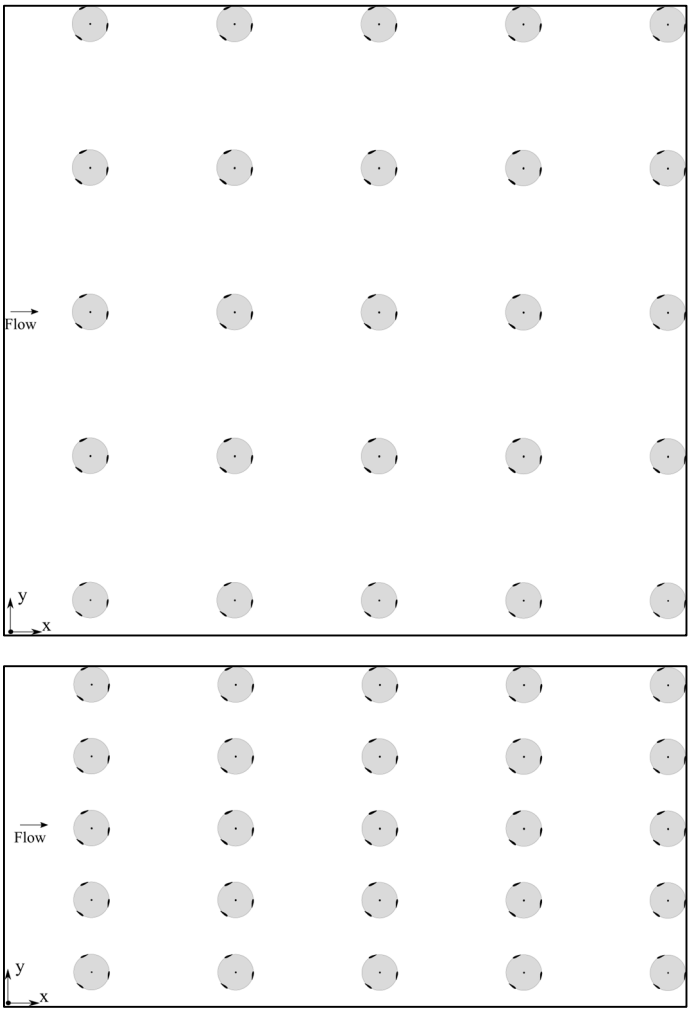

Figure 2 Top view of example wind farms comprising vertical axis turbines with five rows of five turbines per row.

3. Turbine specification and flow conditions

The efficiency of wind farms comprising horizontal and vertical axis turbines is compared considering the SeaTwirl 10MW and DTU 10MW RWT. Both devices have a rated power of 10MW at 11.4 m/s but differ in rotor swept area (A, see Table 1). In case of the horizontal axis turbine, their rotor swept area is circular and has a value of $A = \pi D^2/4$; whilst vertical axis turbines (VATs) feature a rectangular cross-sectional area equal to $A = HD$, with D and H being the rotor diameter and height, respectively. VATs have the particularity of featuring different aspect ratios D/H that yield the same swept area. Varying this rotor aspect ratio would enable to diminish wake losses when H is higher than D as wake recovers faster over the vertical direction.

To enable a robust comparison between rotors, especially when changing the VAT rotor aspect ratio, we define the normalised turbine diameter as $D_0 = A^{0.5}$. Note that in the comparison between HAT and VAT the D_0 of the former is consider for both cases.

Table 1 Details of the geometry characteristics from the rotors of the DTU 10WM RWT and SeaTwirl 10MW turbine.

	DTU 10MW RWT	SEATWIRL 10MW		
A	24,969 m^2	28,880 m^2		
D_0	158.0 m	170 m		
D/H	-	0.5	1.0	2.0
D	178.3 m	120 m	170 m	190 m
H	-	240 m	170 m	152 m
Z_{HUB}	119 m	145 m	110 m	101 m
U_{IN}	4.0 m/s	4.0 m/s		
U_{RATED}	11.4 m/s	11.4 m/s		
U_{OUT}	25.0 m/s	25.0 m/s		

Table 2 presents the power (in MW) estimated to be generated by each turbine rotor respectively, together with its power and thrust coefficients, which are also shown in Figure 3.

Table 2 Power and coefficients of performance and thrust from the SeaTwirl 10MW and DTU 10MW RWT turbines.

TURBINE	**DTU 10MW RWT**			**SEATWIRL 10MW**		
U_{hub} [m/s]	Power [MW]	C_P [%]	C_t [%]	Power[MW]	C_P [%]	C_t [%]
4	0.241	0.246	0.139	0.226	0.200	0.775
6	1.534	0.464	0.687	1.337	0.350	0.759
8	3.765	0.481	0.866	3.623	0.400	0.744
10	7.458	0.488	0.952	7.076	0.400	0.716
12	10.0	0.378	0.601	10.0	0.382	0.701
14	10.0	0.238	0.320	10.0	0.206	0.575
16	10.0	0.160	0.201	10.0	0.138	0.460
18	10.0	0.112	0.137	10.0	0.097	0.380
20	10.0	0.082	0.098	10.0	0.071	0.327

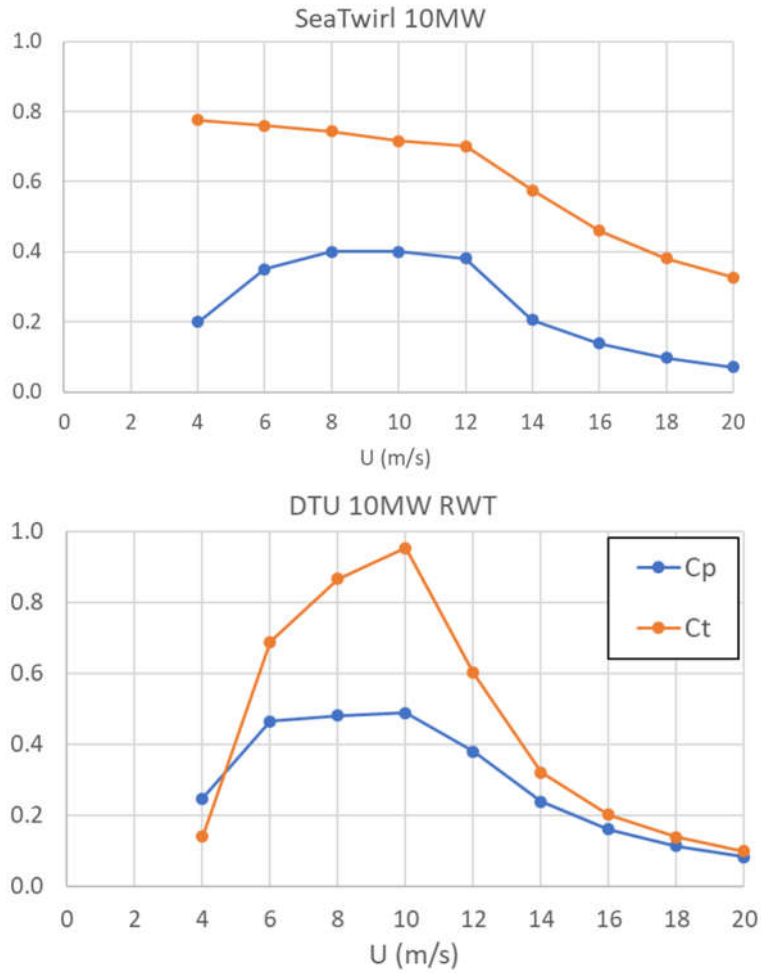

Figure 3 Power and thrust coefficient curves for the SeaTwirl 10MW turbine (top) and DTU 10 MW RWT turbine (bottom).

Offshore wind conditions of Turbulence Class 0A following the DNVGL-ST-0437 and IEC 61400-1 standards are considered. The vertical distribution of the wind profile is set to a power law with a $1/7^{th}$ exponent, such as:

$$U(z) = U(z_r)\left(\frac{z}{z_r}\right)^{1/7} \tag{7}$$

where

$U(z)$ is the wind speed at height z,

z is the height above the still water level,

z_r is a reference height above the still water level used for fitting the profile.

Table 4 presents the estimated probability (provided by SeaTwirl) from occurring of nine hub velocities (U_{hub}) together with the associated turbulence intensity and roughness height (z_o). Note that the DNVGL-ST-0437 and IEC 61400-1 standards state that for turbulence Class 0A the turbulence intensity (TI) is 12% or higher, but this has been considered as too high based on field observations reported at numerous offshore sites such as at Horns Rev wind farm (Barthelmie and Jensen 2010; Hansen et al. 2012). Thus, we modified these turbulence intensity values accordingly otherwise higher turbulence intensity would lead to an underestimation of the wake recovery and thus their negative effects could be wrongly captured.

For the comparison between HAT and VAT farms, all the velocities indicated in Table 3 are considered. Alternatively, only the velocity magnitudes investigated in the comparison between VAT layouts are: 6 m/s, 12 m/s and 18 m/s, which represent scenarios below, at and over rated speed. As wake effects vary depending on the incident flow direction, a total of seven wind directions, namely 0º, 15º, 30º, 45º, 60º, 75º and 90º. are investigated and they are assigned an equal probability in the following analysis.

Table 3 Description of the flow conditions

U_{hub} [m/s]	TI [%]	z_0 [m]	PROBABILITY [%]	HOURS PER YEAR
4	9.0	0.000011	11.00	
6	**8.0**	**0.000028**	**14.12**	**3525**
8	8.0	0.000055	15.12	
10	7.5	0.000091	14.27	
12	**7.5**	**0.000140**	**12.14**	**3140**
14	7.5	0.000200	9.44	
16	8.0	0.000270	6.75	
18	**8.0**	**0.000365**	**4.46**	**1222**
20	8.0	0.000470	2.74	
OTHER	-	-	9.96	**872**

DIRECTION [^{O}]	PROBABILITY [%]
0	14.30
15	14.30
30	14.30
45	14.30
60	14.30
75	14.30
90	14.30

4. Wind farm layouts

The wind farm assessment is carried out for a hypothetical layout comprising a total of 25 turbines divided into five rows of five turbines each. The spacing between the turbines in the streamwise (S_x) and spanwise or transverse (S_y) direction is varied. Details of the proposed layouts are presented in Table 4, with those shown in Figure 2 corresponding to layouts 1 and 3, respectively.

Table 4 Specifications of the wind farm layouts analysed

FARM LAYOUT	S_x/D_0	S_y/D_0	$S_{eq} = (S_xS_y)^{0.5}/D_0$
1	5	5	5.00
2	5	3	3.87
3	5	2	3.16
4	8	8	8.00
5	8	5	6.32
6	8	3	4.90
7	12	8	9.80
8	12	5	7.75
9	12	3	6.00

Complementary characteristics of the wind farm layouts are shown in Table 5, which presents the turbine density for the HAT and VAT layouts that accounts for the mean land surface per turbine, i.e. how densely packed the turbines are; the Installed Capacity Density (ICD) that is analogous to the density but taking into account the installed power instead of number of turbines; and the area occupied by the wind farm extension.

Table 5 Values of the wind farm density, installed capacity density (ICD) and occupied farm area.

LAYOUT	DENSITY [N_T/km^2]	ICD [MW/km^2]	FARM AREA [km^2]
1	1.39	13850	18.05
2	2.31	23084	10.83
3	3.46	34626	7.22
4	0.54	5410	46.21
5	0.87	8657	28.88
6	1.44	14428	17.33
7	0.36	3607	69.31
8	0.58	5771	43.32
9	0.96	9618	25.99

5. Results

The power generated by the turbines is calculated according to Equation 6 in which ρ is the density of the air 1.255 kg/m^3, C_p is the power coefficient shown in Table 2, U_i is the rotor-averaged wind speed and A is the rotor swept area.

$$P_i = \frac{1}{2}\rho\, C_p \int_A U_i^3\, dA \tag{6}$$

The estimated yearly energy yield generated by the DTU 10MW turbine and SeaTwirl's turbine with three rotor aspect ratios is computed based on the results for wind velocities from 4 m/s until 20 m/s and considering an even probability for the seven flow directions considered (see Table 3). Energy yield results in GWh are presented in Table 6 for the proposed layouts and also a case in which no wake effects are computed that resulted from the simulation of a single turbine multiplied by 25 devices as in the other farms.

Table 6 Yearly energy generation in GWh from VAT (E_V) and HAT (E_H).

LAYOUT	E_H [GWh]	E_V [GWh]	E_V [GWh]	E_V [GWh]
D/H	**-**	**1.25**	**1.0**	**0.5**
1	1028	1151	1182	1242
2		1056	1099	1222
3		933	1033	1201
4	1075	1227	1234	1293
5		1200	1217	1278
6		1136	1171	1255
7	1103	1268	1272	1310
8		1245	1255	1288
9		1168	1192	1279
NO WAKES	1177	-	1335	-

Figure 4 shows the values of energy output obtained for the wind farms with HATs and VATs. Overall, the larger the spacing between turbines the higher is their energy output. However, this requires an economic analysis that accounts for cabling and maintenance costs, mooring design or even considerations from the consenting.

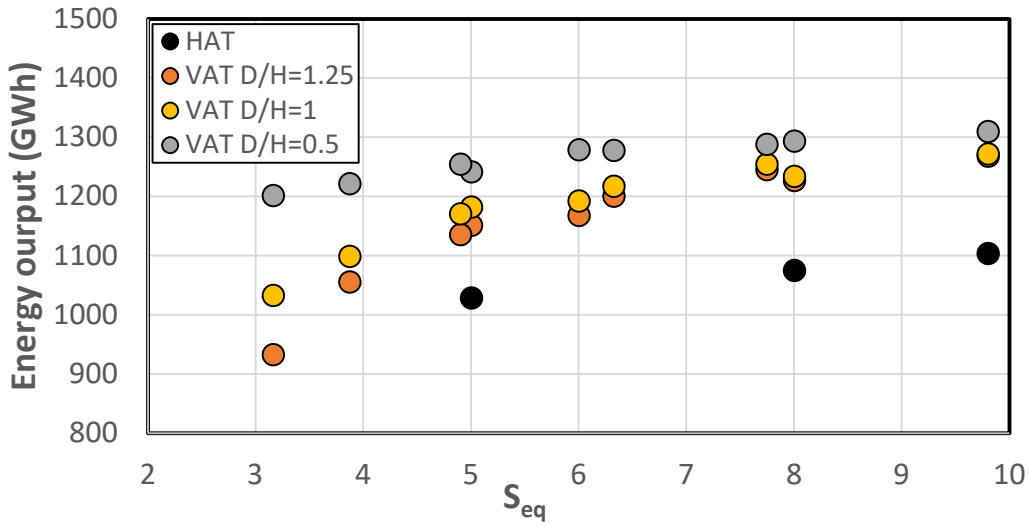

Figure 4 Energy output in GWh estimated to be produced from offshore wind turbine arrays using HAT or VATs with various aspect ratios D/H.

Efficiency as a measure of wake losses

The efficiency of the wind farm can be defined as the mean energy yield performance generated by all turbines (Table 6) compared to that if all operated at rated power at all times, i.e. it is a measure that accounts for the losses derived from wake effects. The farm efficiency is defined in Equation 7 and the obtained results for the different layouts is presented in Table 7. Note the maximum energy yield for the 25 turbines is: 25·10MW·8760h = 2190 GWh. Results show that SeaTwirl VATs consistently experience a reduced impact of the wake effects on their performance, with their efficiency being always above that of HATs. Results from the no-wake scenario represent the capacity factor for the flow conditions indicated in Table 3.

$$\eta = \frac{\sum_{t=1}^{T} E_{tot}(t)}{E_{tot}\ (rated\ capacity)} \tag{7}$$

Table 7 Results of the wind farm efficiency for the different rotor designs and proposed layouts.

LAYOUT	η_H [%]	η_V [%]	η_V [%]	η_V [%]
D/H	**-**	**1.25**	**1.0**	**0.5**
1	47.6	53.3	54.7	57.5
2	-	48.9	50.9	56.6
3	-	43.2	47.8	55.6
4	49.8	56.8	57.1	59.9
5	-	55.6	56.4	59.2
6	-	52.6	54.2	58.1
7	51.1	58.7	58.9	60.6
8	-	57.7	58.1	59.6
9	-	54.1	55.2	59.2
NO WAKES	54.5	-	61.8	-

The previous efficiency results average the power performance for all seven wind directions considered, which are given equal probability (Table 3). An example of how the wind direction drives wind farm performance is presented in Figure 5.

Power Density capacity

Mean power density accounts for how much power is generated considering the occupied land area. This is an important measure as it indicates how efficient the technology is to harness energy from within confined regions, e.g. limited by consented permits. The mean power density (*PD*) is defined in Equation 8 and the results obtained for the different wind farm layouts with HATs and VATs are presented in Table 8.

$$PD = \frac{1}{S_x S_y}\frac{1}{2}\rho A U_0^3 C_p \eta = \frac{P_0}{S_x S_y}\,\eta \tag{8}$$

The higher capability of VATs to harness energy from the wind is well indicated by the *PD* whose values are consistently higher than for HAT farms. For instance, layout 1 with normalised spacing of $5D_0$ in both horizontal directions provided a PD of 6.50 MW/km^2 for HATs whilst this is 7.28 MW/km^2, 7.48 MW/km^2 and 7.85 MW/km^2 for VATs with aspect ratios D/H = 1.25, 1.0 and 0.5, respectively.

Table 8 Power Density results for DTU 10MW RWT turbine (PD_H) and SeaTwirl's 10MW device (PD_V).

LAYOUT	PD_H [MW/km^2]	PD_V [MW/km^2]	PD_V [MW/km^2]	PD_V [MW/km^2]
D/H	**-**	**1.25**	**1.0**	**0.5**
1	6.50	7.28	7.48	7.85
2	-	11.12	11.58	12.87
3	-	14.74	16.33	18.98
4	2.65	3.03	3.05	3.19
5	-	4.74	4.81	5.05
6	-	7.48	7.71	8.26
7	1.82	2.09	2.10	2.16
8	-	3.28	3.31	3.39
9	-	5.13	5.24	5.61

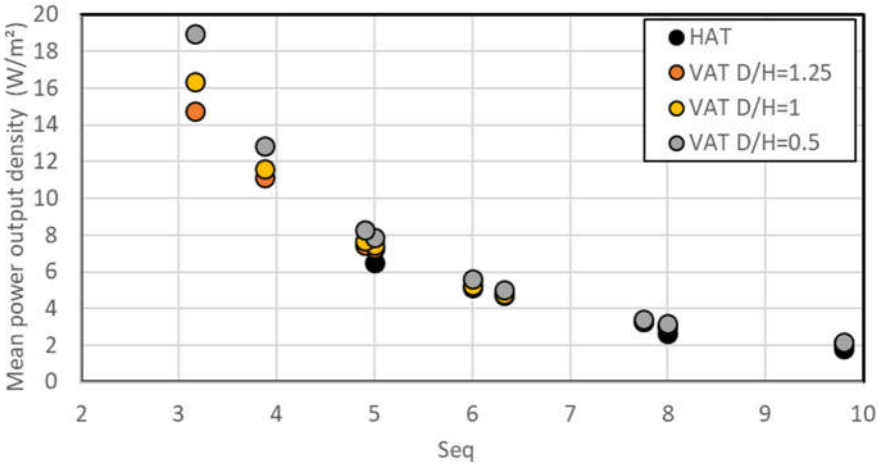

Figure 5 Power Density (PD) capacity results for the HAT and VAT arrays.

Flow directionality: effect on wake development

The energy yield of the wind farm varies with the flow direction as wake effects change. Figure 7 provides the energy generated by the HAT and VAT with D/H = 1.0 layouts when the wind blows at 12 m/s for the different wind directions analysed. VATs outperform HATs for all cases as they operate with a lower thrust coefficient in the region of rated speed (Figure 3) that diminishes wake losses. This figure indicates that for a streamwise spacing of S_x = 12 the wind farm becomes more insensitive to the wind direction than in the other farm arrangements.

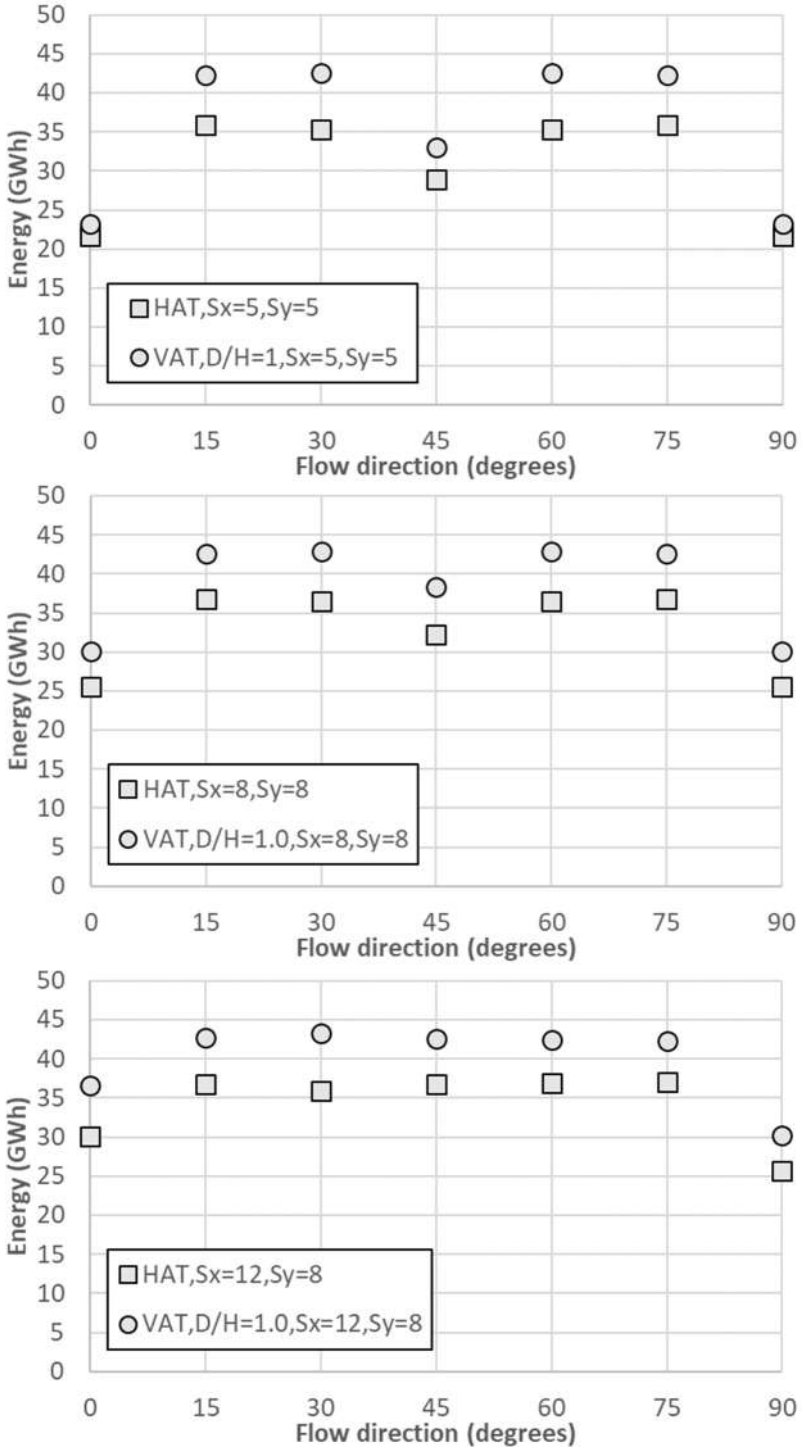

Figure 6 Energy generation for the different HAT and VAT D/H=1.0 layouts at U = 12m/s.

The variation in energy generation in GWh with wind direction and speed between HAT and VAT are presented in figure 7 for layouts 1, 4 and 7. The largest improvement in energy yield from VATs is in the range of 10-14 m/s owed to the lower thrust coefficient that diminishes wake losses. Minimum energy generation is for 0º, 45º and 90º degrees as that correspond to when wakes fully impinge downstream turbines.

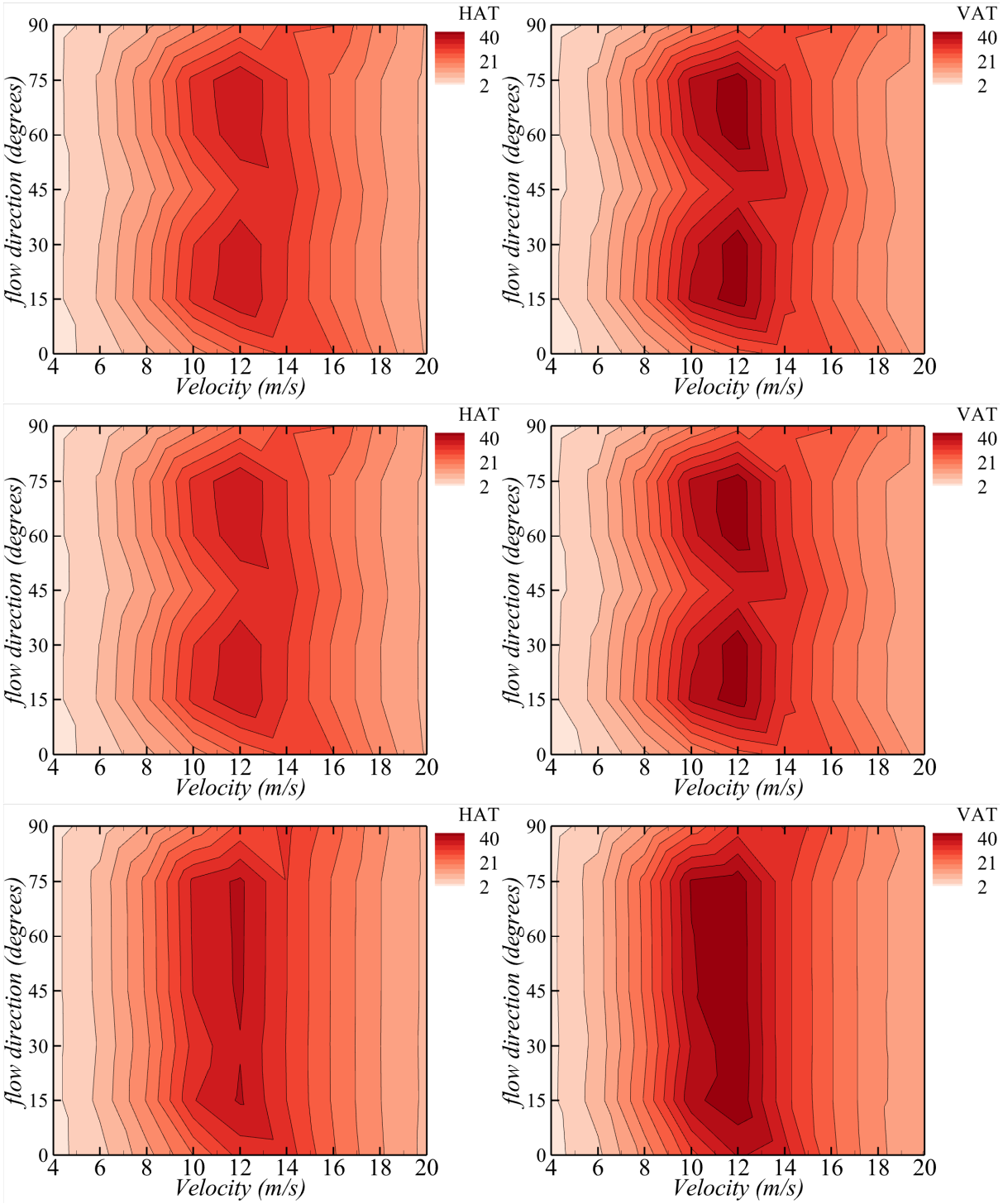

Figure 7 Energy yield in GWh variation with velocity and flow direction obtained for layout 1 (top), 4 (middle) and 7 (bottom) comprising HAT and VAT D/H=1 turbines.

Looking at the influence of the VAT aspect ratio D/H in Figure 8, for D/H = 1.25 the maximum energy generation (when wake effects are lowest) adopting layout 1 corresponds to wind directions of 15 and

75 degrees, whilst for layout 3 this is for 45 degrees. Layout 2 reaches its maximum efficiency for 60 degrees. Similar results are observed for D/H=1.0 aspect ratio. However, for D/H=0.5, the turbines appear less sensitive to the flow direction as the rotor is more slender.

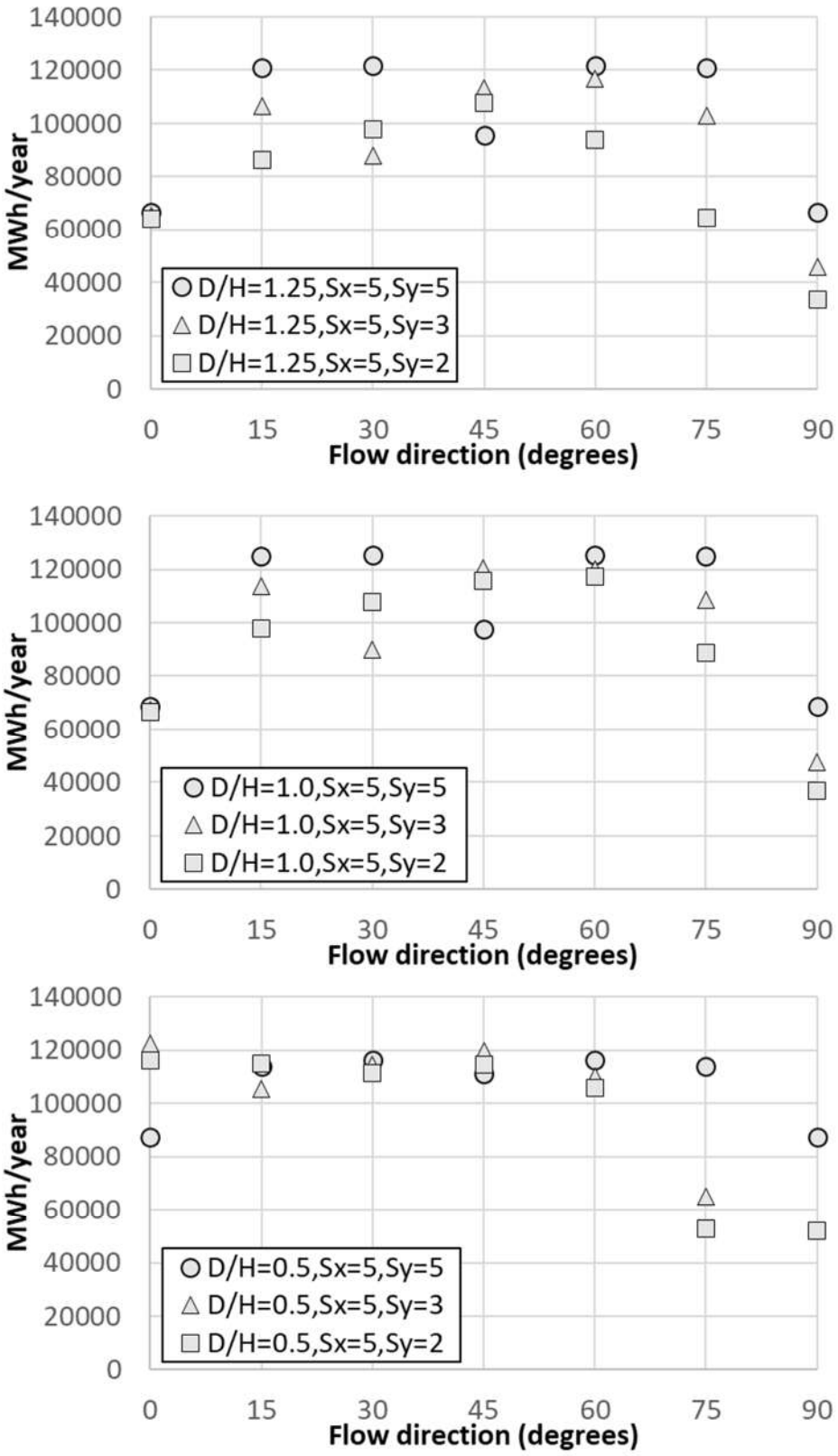

Figure 8 Effect of wind direction on the wind farm energy yield for layouts 1 to 3 with SeaTwirl 10MW turbines and aspect ratios D/H = 1.25 (top), 1.0 (middle) and 0.5 (bottom).

Figures 7 to 13 present the velocity field for the layout 1 using DTU's HAT and SeaTwirl's VAT with *D/H* = 1.0 for the seven flow directions considered at a wind speed of 6m/s. For all cases it can be seen that the VATs recover their wakes faster.

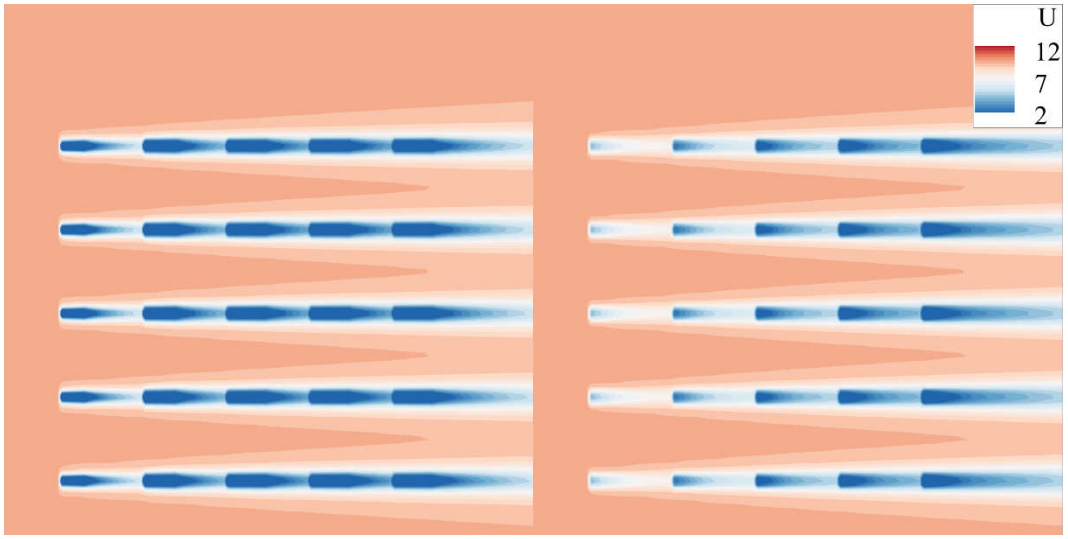

Figure 9 Velocity field computed from layout 1 (S_x/D_0=5, S_y/D_0=5) with DTU 10MW (left) and SeaTwirl 10MW D/H=1.0. Flow velocity is 12 m/s at hub height, and incidence angle is 0º.

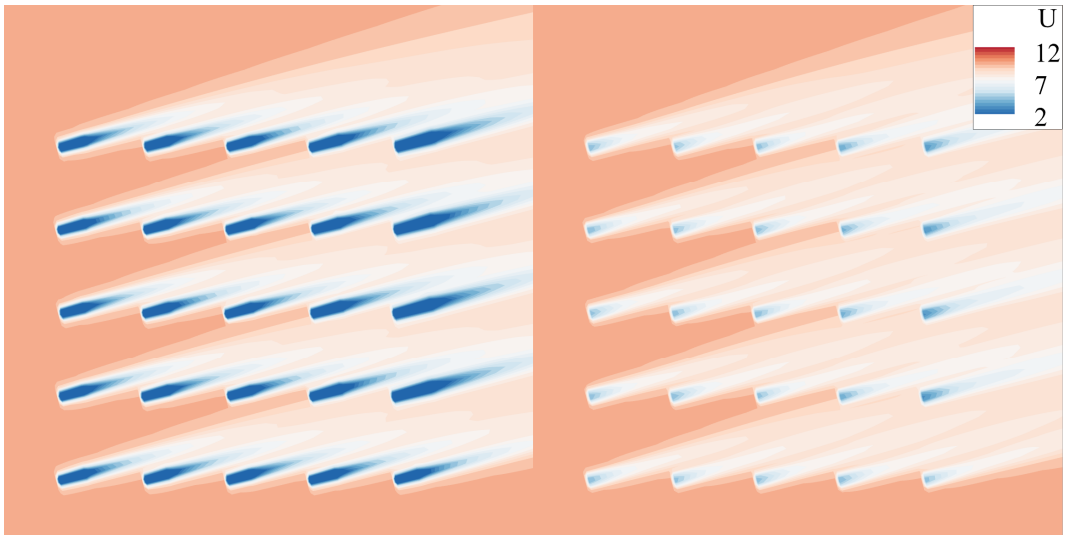

Figure 10 Velocity field computed from layout 1 (S_x/D_0=5, S_y/D_0=5) with DTU 10MW (left) and SeaTwirl 10MW D/H=1.0. Flow velocity is 12 m/s at hub height, and incidence angle is 15º.

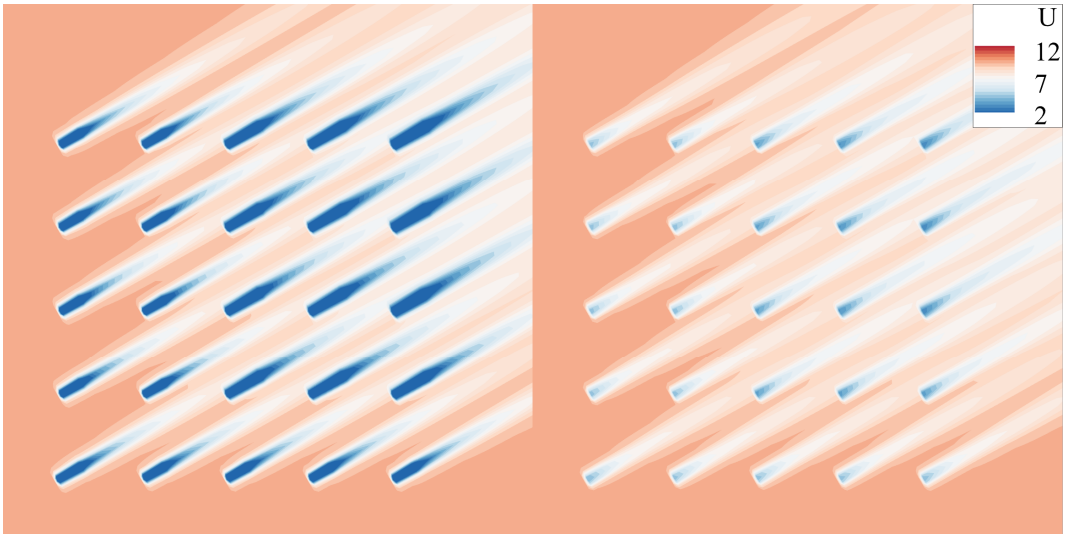

Figure 11 Velocity field computed from layout 1 (S_x/D_0=5, S_y/D_0=5) with DTU 10MW (left) and SeaTwirl 10MW D/H=1.0. Flow velocity is 12 m/s at hub height, and incidence angle is 30º.

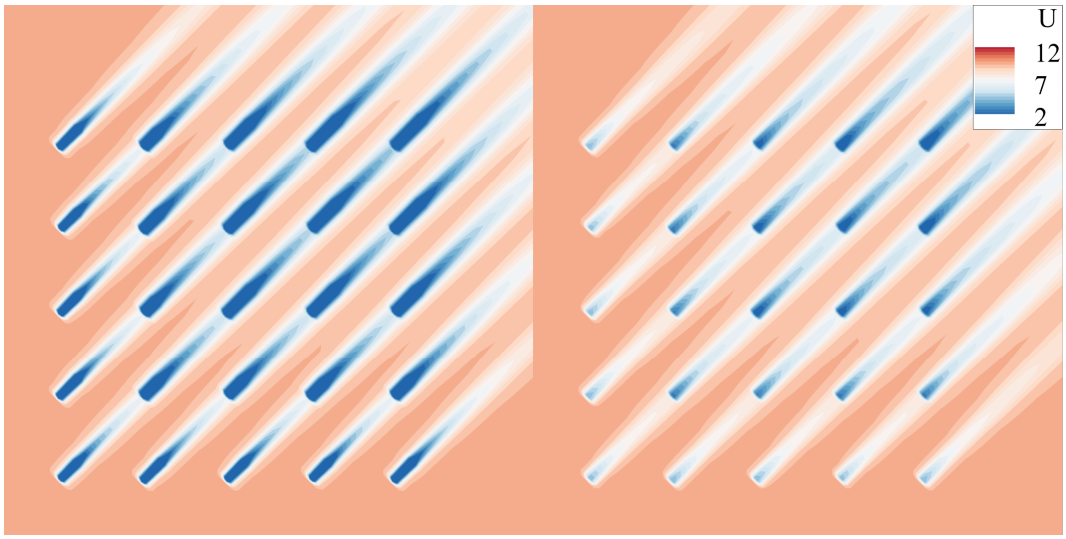

Figure 12 Velocity field computed from layout 1 (S_x/D_0=5, S_y/D_0=5) with DTU 10MW (left) and SeaTwirl 10MW D/H=1.0. Flow velocity is 12 m/s at hub height, and incidence angle is 45º.

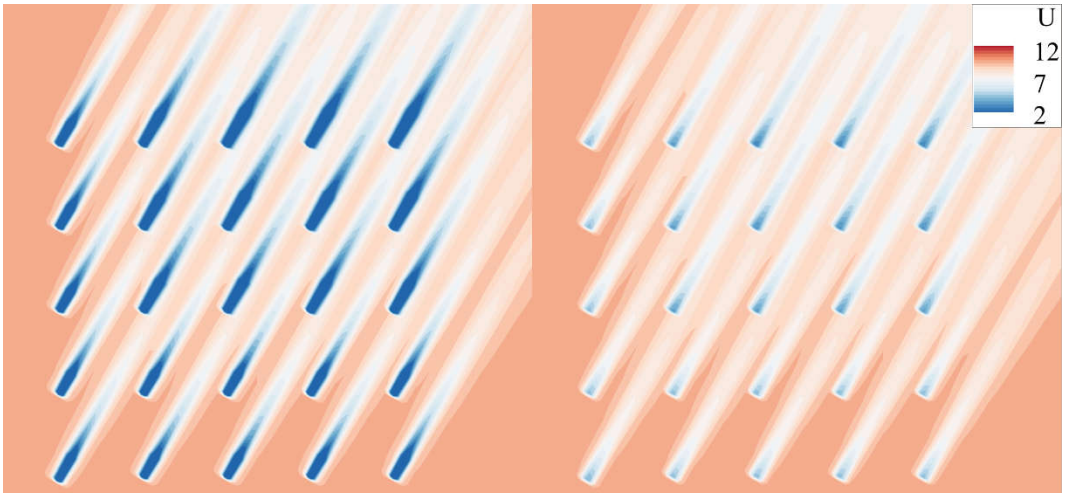

Figure 13 Velocity field computed from layout 1 (S_x/D_0=5, S_y/D_0=5) with DTU 10MW (left) and SeaTwirl 10MW D/H=1.0. Flow velocity is 12 m/s at hub height, and incidence angle is 60º.

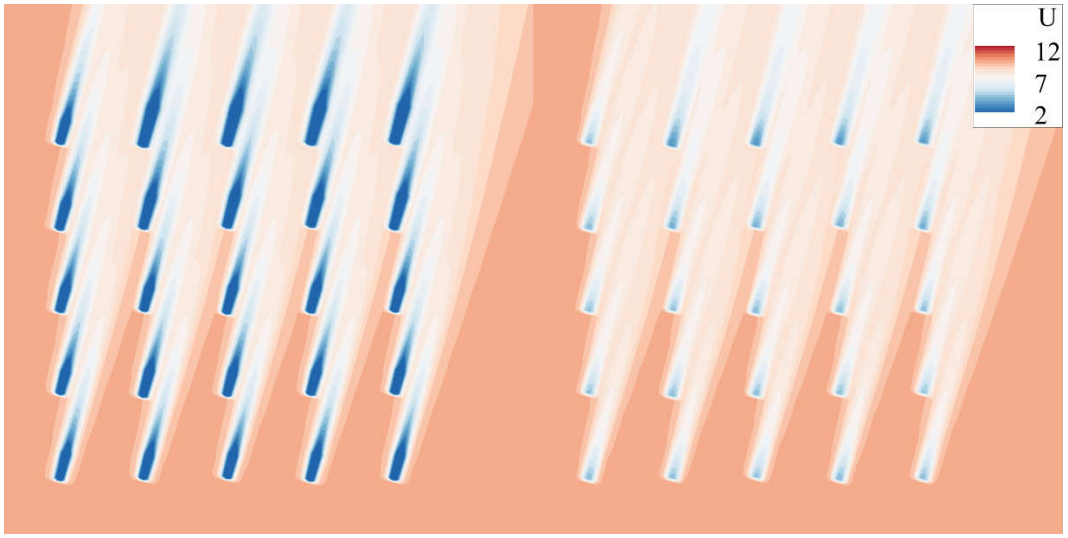

Figure 14 Velocity field computed from layout 1 (S_x/D_0=5, S_y/D_0=5) with DTU 10MW (left) and SeaTwirl 10MW D/H=1.0. Flow velocity is 12 m/s at hub height, and incidence angle is 75º.

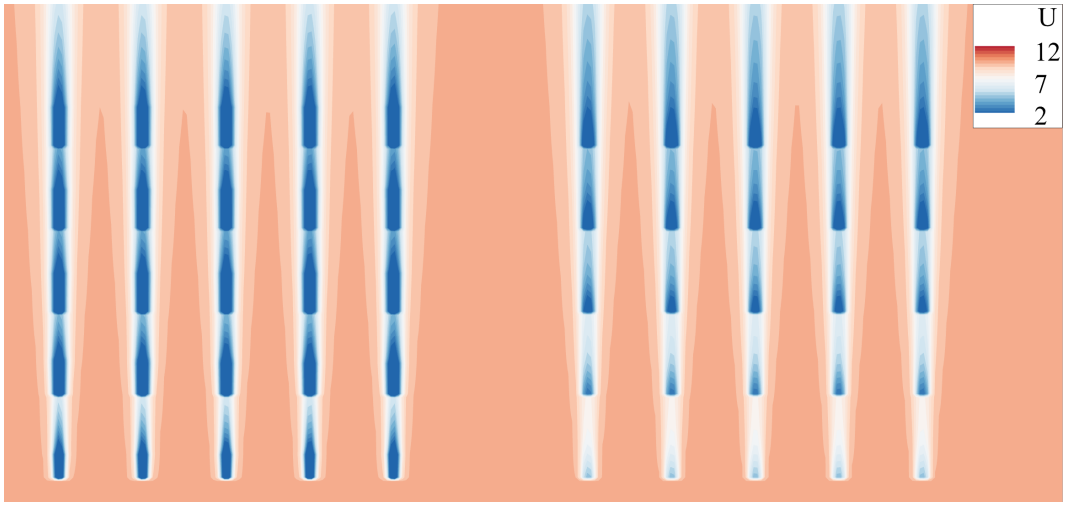

Figure 15 Velocity field computed from layout 1 (S_x/D_0=5, S_y/D_0=5) with DTU 10MW (left) and SeaTwirl 10MW D/H=1.0. Flow velocity is 12 m/s at hub height, and incidence angle is 90º.

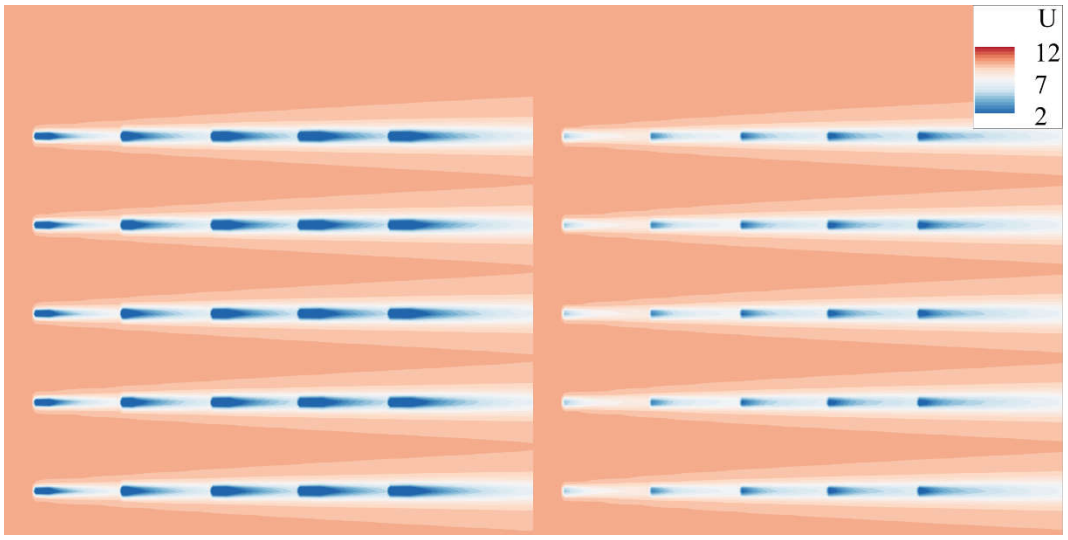

Figure 16 Velocity field computed from layout 1 (S_x/D_0=8, S_y/D_0=8) with DTU 10MW (left) and SeaTwirl 10MW D/H=1.0. Flow velocity is 12 m/s at hub height, and incidence angle is 0º.

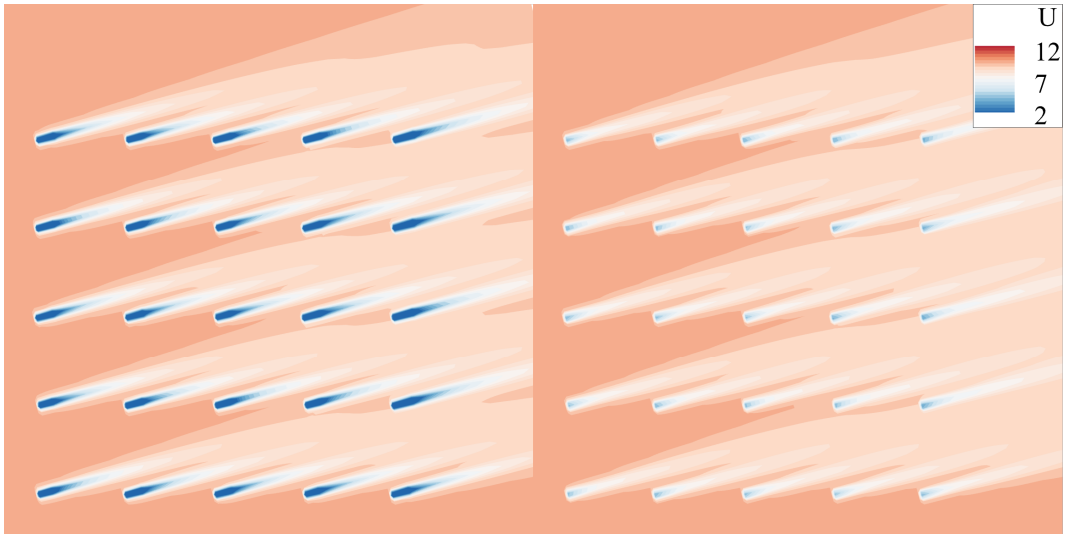

Figure 17 Velocity field computed from layout 1 (S_x/D_0=8, S_y/D_0=8) with DTU 10MW (left) and SeaTwirl 10MW D/H=1.0. Flow velocity is 12 m/s at hub height, and incidence angle is 15º.

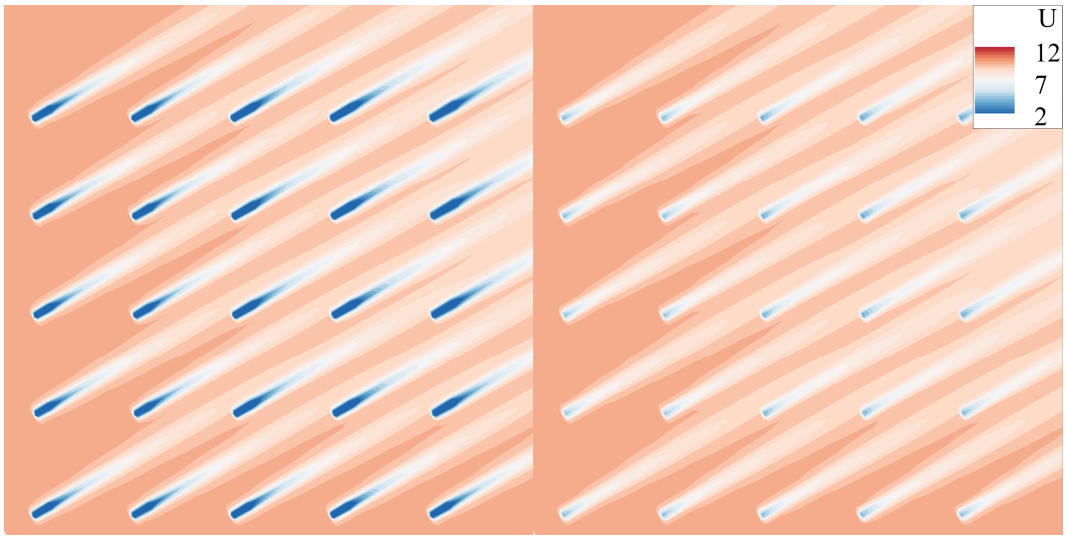

Figure 18 Velocity field computed from layout 1 (S_x/D_0=8, S_y/D_0=8) with DTU 10MW (left) and SeaTwirl 10MW D/H=1.0. Flow velocity is 12 m/s at hub height, and incidence angle is 30º.

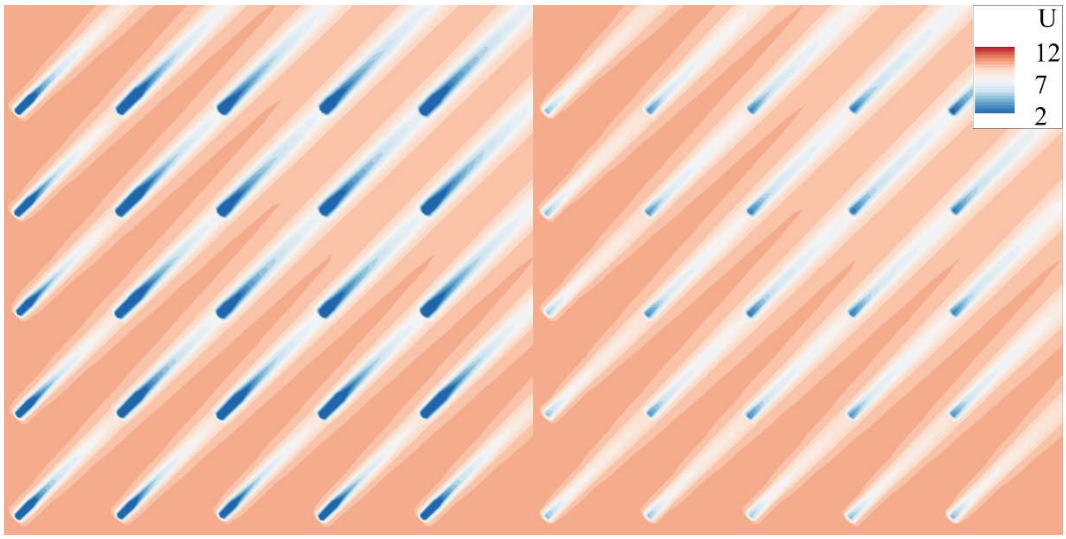

Figure 19 Velocity field computed from layout 1 (S_x/D_0=8, S_y/D_0=8) with DTU 10MW (left) and SeaTwirl 10MW D/H=1.0. Flow velocity is 12 m/s at hub height, and incidence angle is 45º.

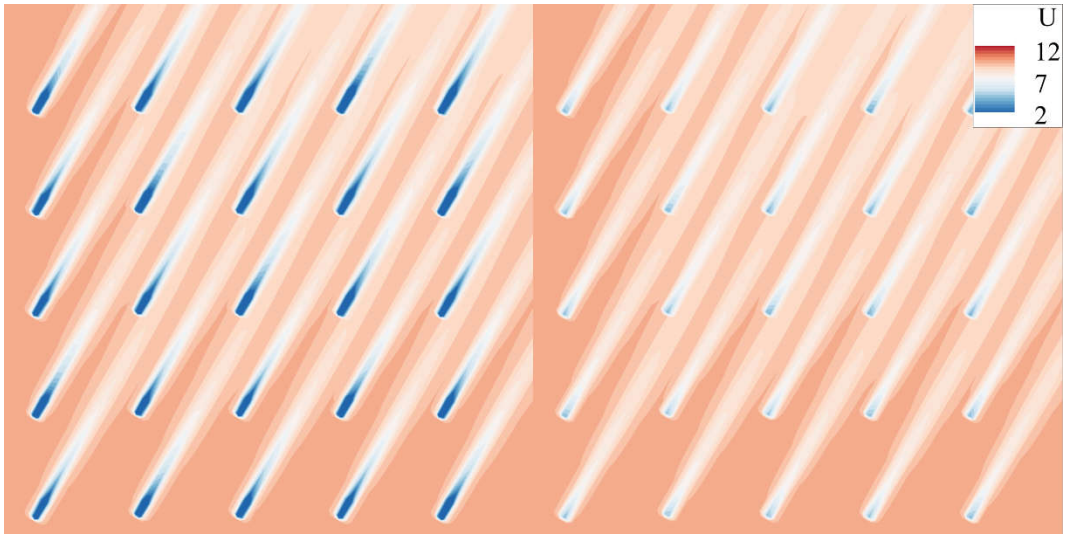

Figure 20 Velocity field computed from layout 1 (S_x/D_0=8, S_y/D_0=8) with DTU 10MW (left) and SeaTwirl 10MW D/H=1.0. Flow velocity is 12 m/s at hub height, and incidence angle is 60º.

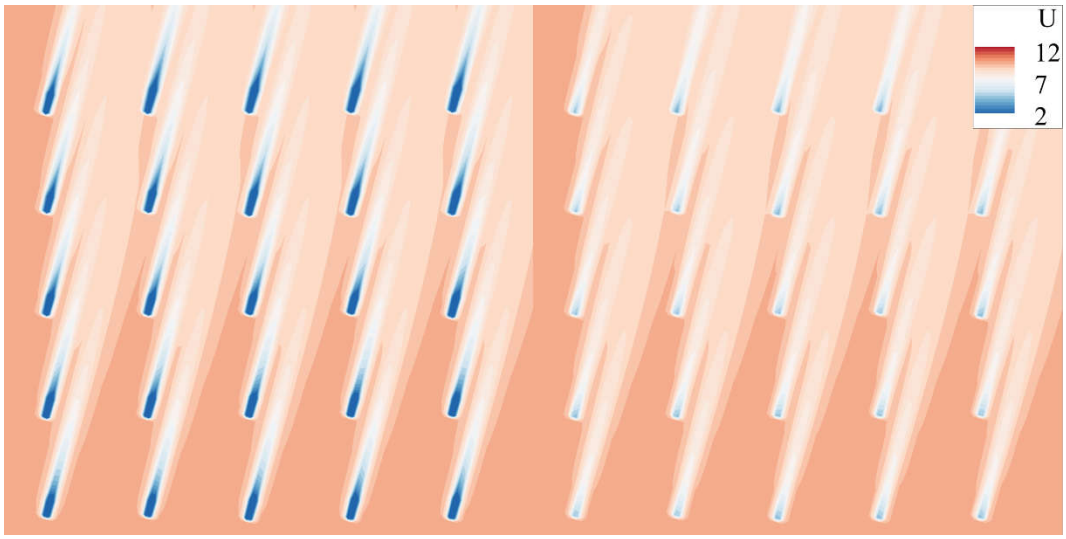

Figure 21 Velocity field computed from layout 1 (S_x/D_0=8, S_y/D_0=8) with DTU 10MW (left) and SeaTwirl 10MW D/H=1.0. Flow velocity is 12 m/s at hub height, and incidence angle is 75º.

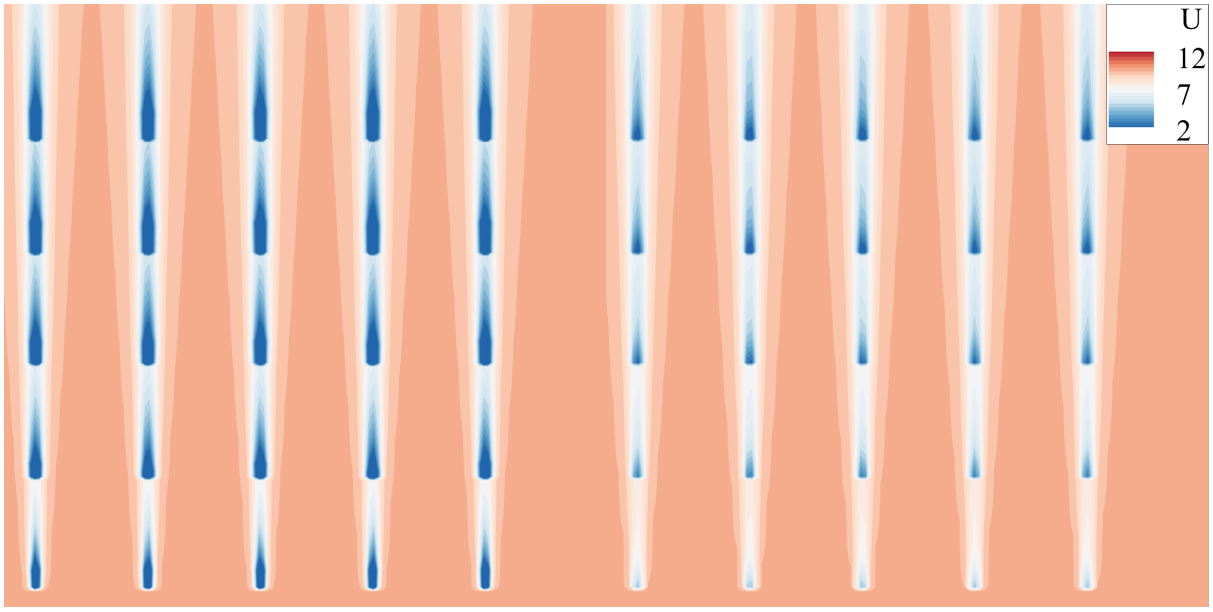

Figure 22 Velocity field computed from layout 1 (S_x/D_0=8, S_y/D_0=8) with DTU 10MW (left) and SeaTwirl 10MW D/H=1.0. Flow velocity is 12 m/s at hub height, and incidence angle is 90º.

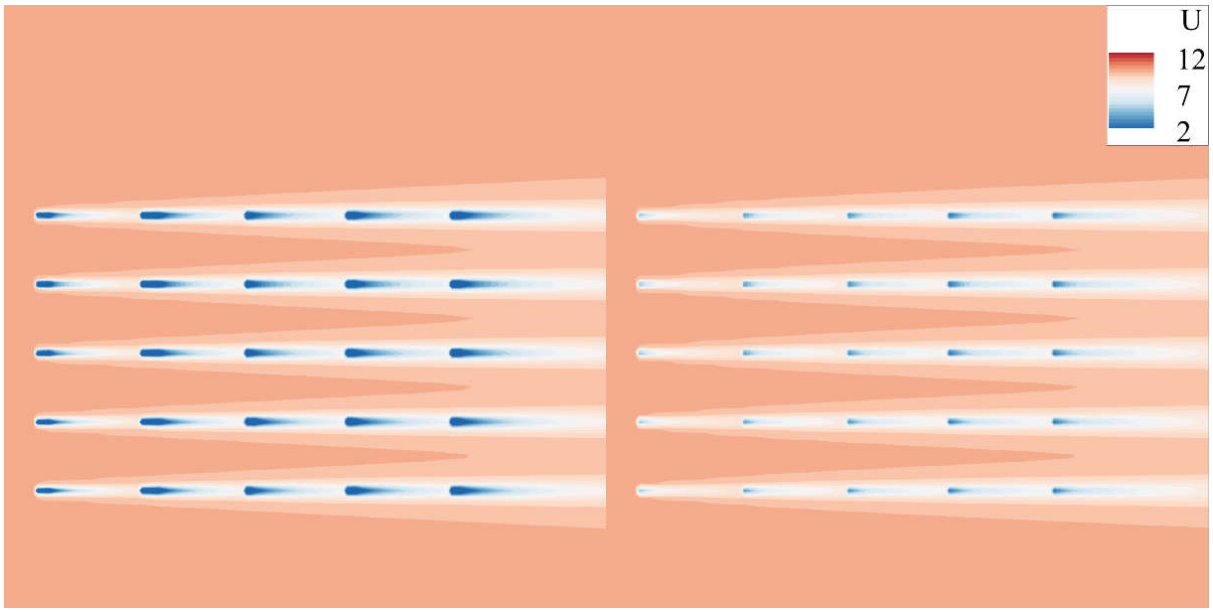

Figure 23 Velocity field computed from layout 1 (S_x/D_0=12, S_y/D_0=8) with DTU 10MW (left) and SeaTwirl 10MW D/H=1.0. Flow velocity is 12 m/s at hub height, and incidence angle is 0º.

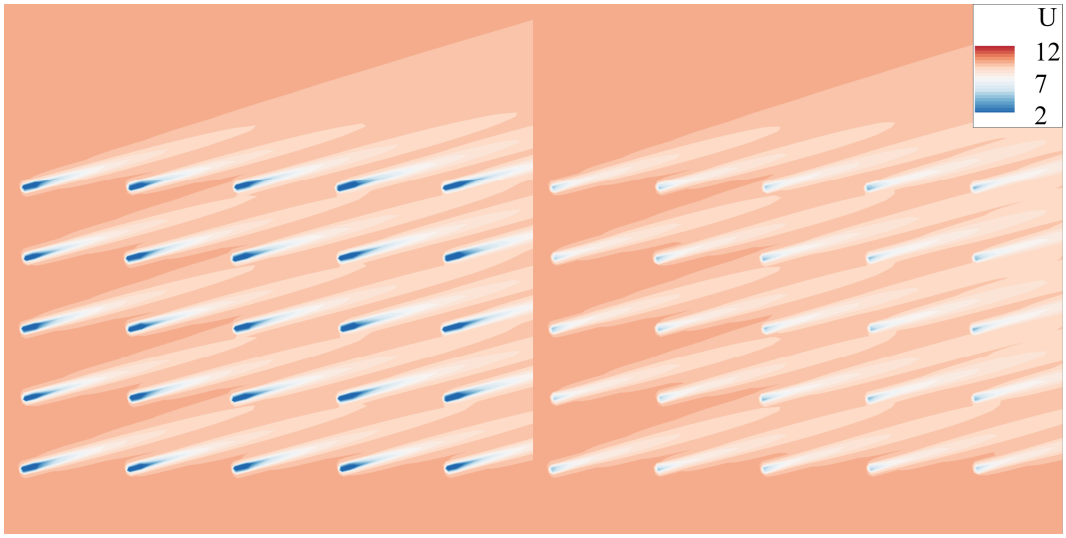

Figure 24 Velocity field computed from layout 1 (S_x/D_0=12, S_y/D_0=8) with DTU 10MW (left) and SeaTwirl 10MW D/H=1.0. Flow velocity is 12 m/s at hub height, and incidence angle is 15º.

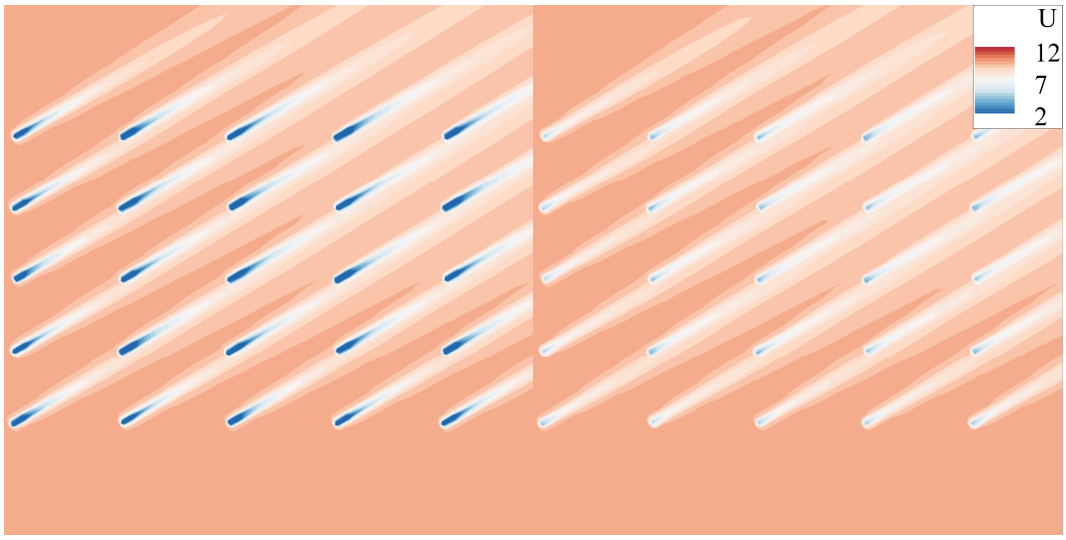

Figure 25 Velocity field computed from layout 1 (S_x/D_0=12, S_y/D_0=8) with DTU 10MW (left) and SeaTwirl 10MW D/H=1.0. Flow velocity is 12 m/s at hub height, and incidence angle is 30º.

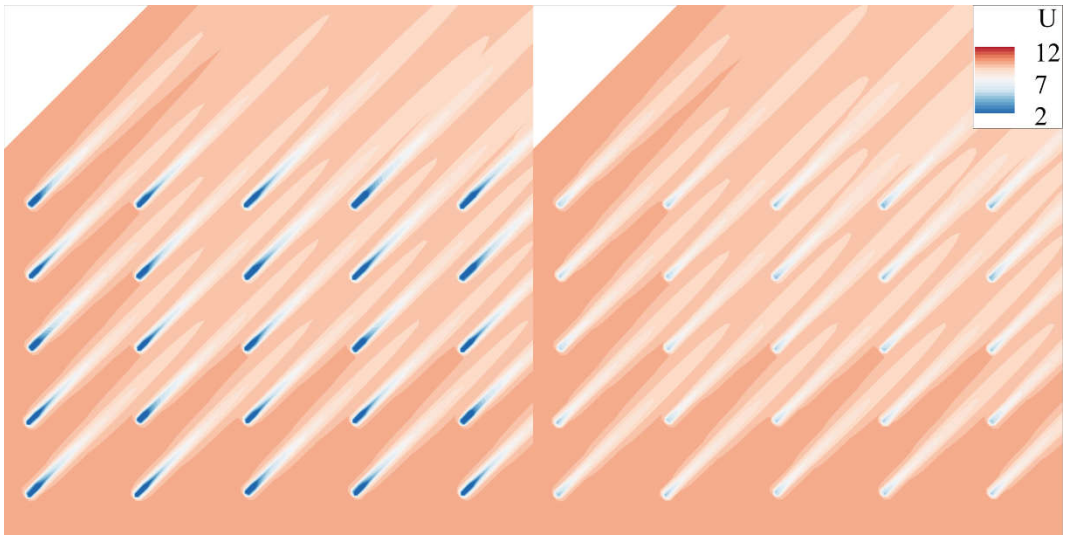

Figure 26 Velocity field computed from layout 1 (S_x/D_0=12, S_y/D_0=8) with DTU 10MW (left) and SeaTwirl 10MW D/H=1.0. Flow velocity is 12 m/s at hub height, and incidence angle is 45º.

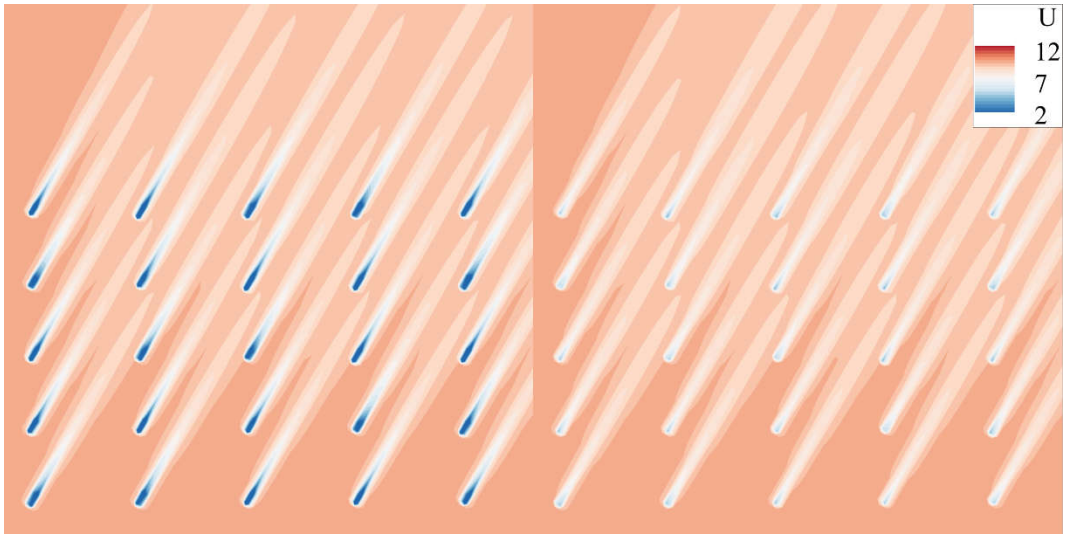

Figure 27 Velocity field computed from layout 1 (S_x/D_0=12, S_y/D_0=8) with DTU 10MW (left) and SeaTwirl 10MW D/H=1.0. Flow velocity is 12 m/s at hub height, and incidence angle is 60º.

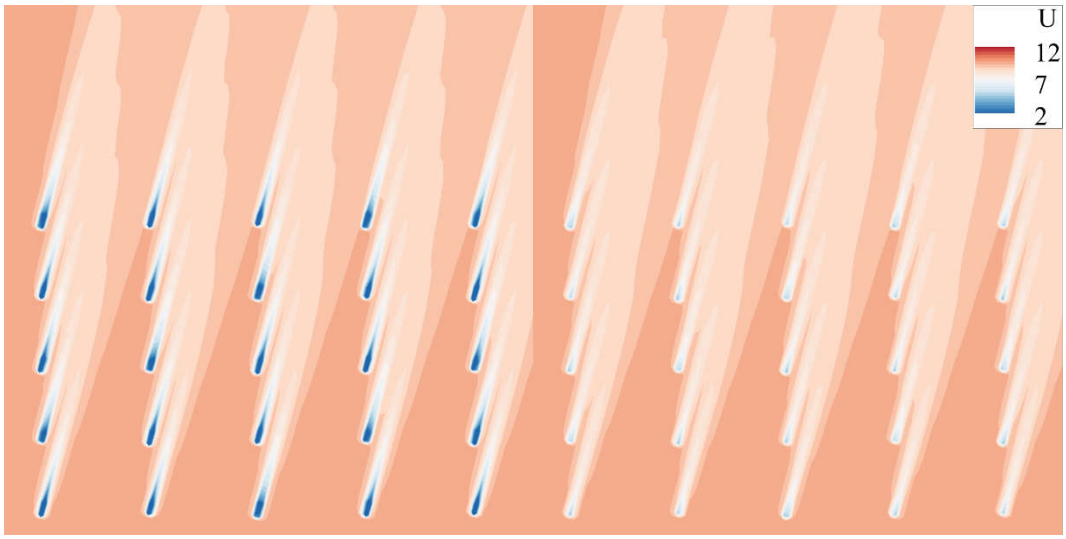

Figure 28 Velocity field computed from layout 1 (S_x/D_0=12, S_y/D_0=8) with DTU 10MW (left) and SeaTwirl 10MW D/H=1.0. Flow velocity is 12 m/s at hub height, and incidence angle is 75º.

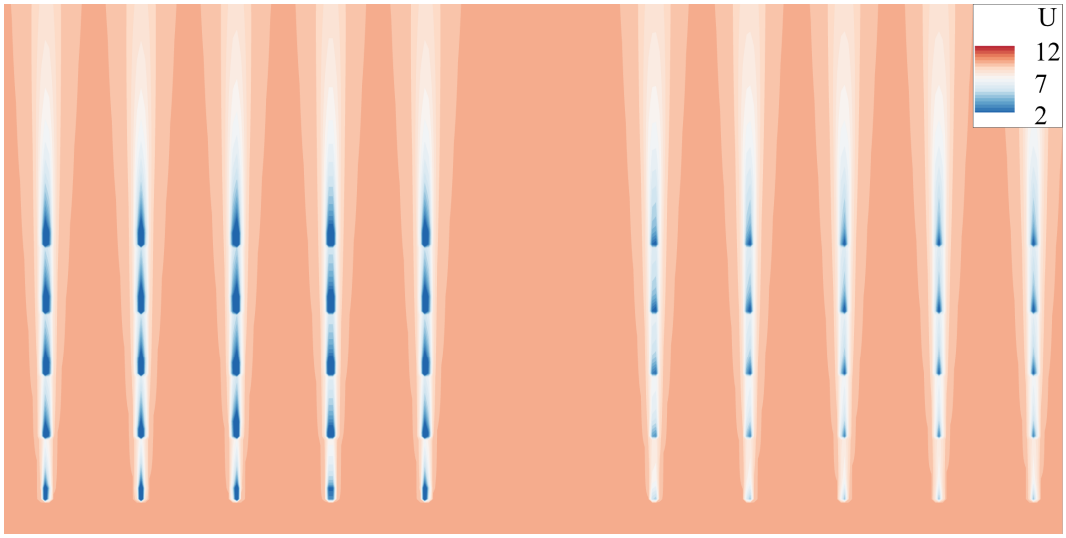

Figure 29 Velocity field computed from layout 1 (S_x/D_0=12, S_y/D_0=8) with DTU 10MW (left) and SeaTwirl 10MW D/H=1.0. Flow velocity is 12 m/s at hub height, and incidence angle is 90°.

6. Conclusions

From the comparison of offshore wind farms comprising 25 10 MW turbines with horizontal (DTU) or vertical axis turbines (SeaTwirl design), VATs outperform HATs in energy yield for most wind conditions due to a lower thrust coefficient at rated speed and faster wake recovery. The direct comparison between HAT and VAT farms for three layouts shows that the VATs provide an average increase of 13%. The energy output of VATs increase if the aspect ratio *D/H* is smaller, i.e. slender VAT rotors reduce wake interactions and increase energy generation. VAT wakes recover faster than HAT wakes due to the different mixing with the atmospheric flows which in turn leads to more efficient arrays.

7. References

Archer et al. 2018. Review and evaluation of wake loss models for wind energy applications. Applied Energy. 226: 1187-1207.

Barthelmie R.J. and Jensen L.E. 2010. Evaluation of wind farm efficiency and wind turbine wakes at the Nysted offshore wind farm. Wind Energy. 13:573–586.

Bastankhah and Porté-Agel. 2014. A new analytical model for wind-turbine wakes. Renewable Energy. 70: 116-123.

Hansen K.S et al. 2012. The impact of turbulence intensity and atmospheric stability on power deficits due to wind turbine wakes at Horns Rev wind farm. Wind Energy. 15:183–196

Ouro and Lazennec. 2021. Theoretical modelling of the three-dimensional wake of vertical axis turbines. 1: E3.

Ouro et al. 2022. Power density capacity of tidal stream turbine arrays with horizontal and vertical axis turbines. Under review.